Remote Sensing of Environment 285 (2023) 113419

Contents lists available at ScienceDirect

Remote Sensing of Environment

journal homepage: www.elsevier.com/locate/rse

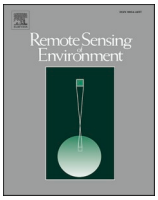

Impact of seasonal fluctuations of ice velocity on decadal trends observed in Southwest Greenland

Paul Halas [a,*], Jérémie Mouginot [b], Basile de Fleurian [a], Petra M. Langebroek [c]

[a] University of Bergen, Bjerknes Centre for Climate Research, Bergen, Norway
[b] Institut des Géosciences de l'Environnement, Université Grenoble Alpes, CNRS, IRD, INP, Grenoble, France
[c] NORCE Norwegian Research Centre, Bjerknes Centre for Climate Research Bergen, Norway

ARTICLE INFO

Edited by Dr. Menghua Wang

Keywords:
Optical remote-sensing
Landsat 7–8
Sentinel-2
Feature-tracking
Ice velocity trends
Southwest Greenland

ABSTRACT

By tracking the feature displacement between satellite images spaced approximately one year apart, surface runoff has been shown to have a long-term impact on the average ice flow of a land-terminating sector of Greenland. In this study, we revisit the multi-year trends in ice flow by assessing more carefully the impact of seasonal fluctuation in velocity on the annual mean ice velocity. We find that, depending on the length and period used to measure displacement, seasonal fluctuations do have an impact on observed velocities on up to 15%, and can affect decadal trends. Nevertheless, the magnitude of this fluctuation is small enough to confirm the general slowdown observed during the 2000–2012 period. Between 2012 and 2019, we find significant re-acceleration of low-lying glaciers tongue but velocity trends elsewhere are generally insignificant and not spatially consistent. Finally, we propose a more selective approach to recovering velocity trends using satellite imagery that involves using only measurements where the image pair starting date is before summer, in order to have comparable measurements for every year, sampling a melt season and the following winter.

1. Introduction

Optical remote sensing for ice velocity mapping has been increasingly used in the past decades and has now proven its versatility in numerous applications (Fahnestock et al., 2016; Millan et al., 2022; Mouginot et al., 2017; Rabatel et al., 2018; Shen et al., 2018; Zhou et al., 2021).

Indeed, these observations are useful to quantify past and present rates of ice sheet mass changes and/or to improve our understanding of the physical processes acting on ice movement, with the interest to predict the evolution of ice masses in a warming climate.

Changes in ice flow have been observed for the Greenland Ice Sheet (GrIS), as well as in mountain glaciers and in West Antarctica (e.g. Dehecq et al., 2019; Joughin et al., 2008; Lilien et al., 2018; Palmer et al., 2011; Parizek and Alley, 2004; Shepherd et al., 2009; Tuckett et al., 2019; Van De Wal et al., 2008, 2015; Zwally et al., 2002).

Studying causes for such ice flow variations requires both geological settings where studied factors are as less entangled as possible, and an area where satellite data is available.

The Southwest of the GrIS provides numerous land-terminating glaciers, which are ideal ice laboratories isolated from ocean-related processes, allowing to study the impact of various factors on the ice dynamics, and are also reasonably covered by satellites for ice velocity mapping (Davison et al., 2019; Derkacheva et al., 2020; Doyle et al., 2014; Joughin et al., 2018; Lemos et al., 2018; Sole et al., 2013; Tedstone et al., 2013, 2015; Williams et al., 2020).

While being isolated from the ocean, land-terminating glaciers are also displaying slower velocities, leading potentially to smaller - i.e. less easily detectable - variations in time. The need to study such ice velocity trends therefore requires a combination of accurate velocity estimations, and long time-series (Joughin et al., 2018; Mouginot et al., 2017; Tedstone et al., 2015; Williams et al., 2020).

To study the long-term impact of surface run-off on ice flow, Tedstone et al. (2015) and Williams et al. (2020) used feature-tracking on Landsat satellite image pairs separated by approximately one year to calculate ice velocities on a land-terminating part of the southwest sector of the GrIS. They identified respectively 475 and 2665 image pairs, covering April to October over the years 1985–2014 for the former, and 1985–2019 for the latter.

The obtained velocity fields were then averaged to give median spatial velocity fields for every year, from which trends over the approximately 30 years could be derived and compared with trends in

* Corresponding author.
E-mail address: paul.halas@uib.no (P. Halas).

https://doi.org/10.1016/j.rse.2022.113419
Received 1 June 2022; Received in revised form 12 December 2022; Accepted 14 December 2022
Available online 19 December 2022

surface run-off.

With these observations, both studies found a long-term impact of the increase in surface melting on the mean ice velocity. Both found a decelerating trend starting around 2002 linked to the increasing surface run-off, and Williams et al. (2020) also found a significant re-acceleration from 2012 to 2019 associated this time with a decrease in surface run-off.

In contrast, Joughin et al. (2018) using a combination of radar and optical data to compute trends with winter velocities, could not confirm the trends established by Tedstone et al. (2015).

These contradictory results highlight the difficulty of determining trends in velocity fields that do not necessarily represent the same period of the year or the same spatial coverage. Thus, given the high seasonal variability of the ice flow in these regions (Derkacheva et al., 2020; Joughin et al., 2018; Moon et al., 2015), aggregating multiple individual measurements made during one year by performing a simple median or mean might result into biased annual velocity values, since the temporal and spatial sampling varies from one year to another.

As underlined by Joughin et al. (2018), a sampling bias is possible in the dataset from Tedstone et al. (2015), since it includes velocity information obtained from images separated by 352 to 400 days. Indeed, the date of the first image ("starting date") used to derive displacements and the time between of the two acquisitions ("temporal baseline") used could lead to a disproportionate sampling of summer when enhanced ice velocities are expected (Derkacheva et al., 2020; Lemos et al., 2018; Maier et al., 2019; Palmer et al., 2011). Thus, trends obtained for "yearly" velocities could potentially differ from trends derived only from winter velocities.

Tedstone et al. (2015) and Williams et al. (2020) argue that combining many velocity measurements obtained at different dates and with different time interval between acquisitions for a given year does not have a significant impact on the estimation of the multi-annual trends.

Tedstone et al. (2015) studied partly this impact by analysing the average date of year of satellite images used, the average baseline duration used, and the proportion of the baseline duration attributable to summer. However, the average start day-of-year does not describe the distribution of image pairs, and different combinations of image pairs can lead to the same average start day-of-year. The same applies to the average baseline duration.

Here, we assess whether the starting date and baseline duration for around one-year image pairs have an impact on the overall velocity derived from these images. This is important as, the previously observed inter-annual trends in velocity are relatively small (-1.5 m/yr^2 for the period 2002–2014 in Tedstone et al. (2015)) compared to the seasonal variations, whose summer accelerations are typically of the order of 100 m/yr. Potential biases caused by the measurement techniques (e.g. mapping speed using one-year pair) should therefore be assessed and reduced as much as possible.

We first describe our processing approach to obtain ice velocity maps from Landsat 8 and Sentinel-2 images acquired about 1 year apart, and compare our results to GPS-derived velocities. We then compute the velocity trends using periods similar to the ones defined in Williams et al. (2020) from 2000 to 2012 and from 2012 to 2019, and discuss the impact of starting date (before, during or after summer) on the mean velocities. Finally, we discuss the significance of deriving mean velocity trends for a whole region, when local variations may be present.

2. Methods

2.1. Study area

Our study area is located in Southwest Greenland and is displayed in Fig. 1. The area is south of Jakobshavn Isbræ and extends around 300 km to the South, and up to 1200 m altitude, covering both study areas of Tedstone et al. (2015) and Williams et al. (2020), but does not cover

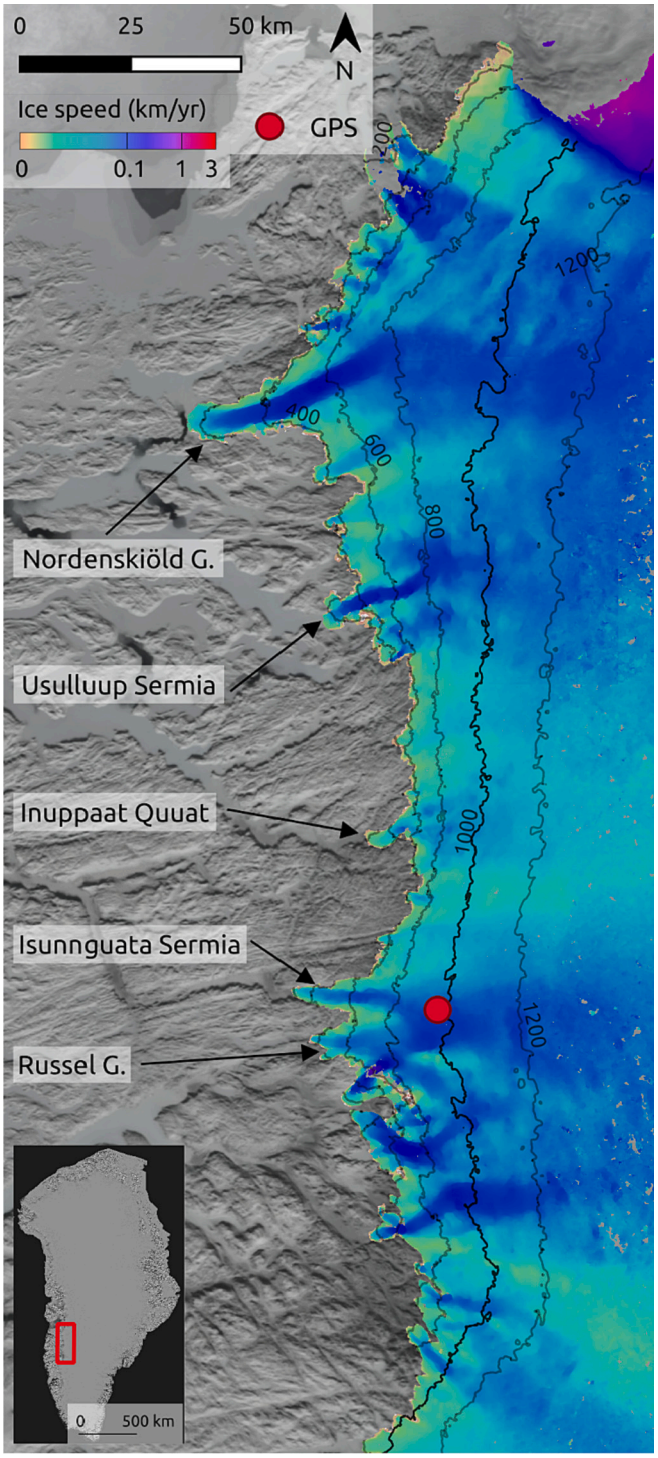

Fig. 1. Map of the study area. Ice velocities displayed are derived by combining all velocity fields computed in this study from image pairs of Landsat 8 and Sentinel-2 for year 2019–2020. The red dot indicates the position of the GPS measurements made by Maier et al. (2019). The ice velocities are overlaying a 2015 MODIS Mosaic of Greenland (MOG) at 100 m resolution (Haran et al., 2018). (For interpretation of the references to colour in this figure legend, the reader is referred to the web version of this article.)

Joughin et al. (2018) study area, which extends much further south. This sector of the Greenland Ice sheet is mostly composed of land-terminating glaciers where it is assumed that changes in ice velocity is mostly controlled by changes in basal conditions (de Fleurian et al., 2016; Derkacheva et al., 2020). The glaciers (Isunnguata Sermia, Russell and

Ørkendalen Gletscher) close to the town of Kangerlussuaq have been extensively studied. Indeed, this sector has been the subject of in-situ geophysical investigations such as mechanical properties of sediment bed underlying the glaciers and their influence on the ice flow (Dow et al., 2013; Harper et al., 2017; Kulessa et al., 2017; Maier et al., 2019; Wright et al., 2016), making it a privileged study site for numerical investigations (Bougamont et al., 2014; Brinkerhoff et al., 2021; de Fleurian et al., 2016; Koziol and Arnold, 2017, 2018). Here, we make use of the precise ice motion measurements obtained on Isunnguata Sermia by GPS between 2014 and 2017 by Maier et al. (2019) (Fig. 1).

2.2. Satellite observations

In order to obtain ice velocities on a large scale, we applied commonly used optical feature-tracking on Landsat 7 (band 8), Landsat 8 (band 8) and Sentinel-2 (band 8) imagery pairs (spatial resolution of 15 m, 15 m (panchromatic) and 10 m (NIR), respectively), taking advantage of persisting features on the surface of the ice between two images to derive displacement maps (following e.g. Dehecq et al., 2015; Fahnestock et al., 2016; Jeong et al., 2017; Joughin, 2002; Millan et al., 2019; Mouginot et al., 2019; Paul et al., 2015; Scambos et al., 1992). The dates of two images used in the feature-tracking are called hereafter the starting and ending dates, while the time interval between the two images is called baseline duration.

The processing chain is the same as used in Millan et al. (2019, 2022); Mouginot et al. (2017, 2019). It is downloading all L1C satellite products from USGS and Copernicus databases in our region of interest, discarding images with cloud coverage above 40%. Image pairs are then defined by matching images from similar orbits and sensors.

A Sobel filter is applied to images in order to enhance surface features (Dehecq et al., 2015; Millan et al., 2019). The processing chain then computes the normalized cross correlation between the two images, with a window size of 64 × 64 pixels chosen for the sub-image, and uses an a priori velocity map in order to guide the correlation (Dehecq et al., 2015). The processing chain uses a modified version of the ampcor algorithm, part of the ROI-PAC package (Millan et al., 2022; Rosen et al., 2004).

We chose optical feature-tracking on images separated by about one year to increase signal to noise ratio and limit the impact of seasonal variations, as done for e.g. in Dehecq et al. (2015) and Tedstone et al. (2015). While being an average of the velocity between the two images, optical feature-tracking with one year temporal baseline also allows for a much greater level of precision compared to shorter baselines, with an expected tracking of features down to 0.1 pixels (Debella-Gilo and Kääb, 2011), as directly shown with the same correlation algorithm in Millan et al. (2019) and Mouginot et al. (2017). Our final dataset ranges from 2000 to 2020, and uses all image pair combinations separated by a baseline of 336–400 days for Landsat, and 335–395 days for Sentinel-2.

Window sizes between 16 × 16 to 128 × 128 pixels have been tested, and correlation was found to be optimal for this region at 64 × 64 size, yielding better coverage for moderate ice velocity (velocities between 50 and 100 m/yr) than smaller windows.

To assist feature tracking, we use a-priori ice displacements from previous velocity maps. This step reduces the search area for pixel offsets at each location to about 4 × 4 pixels in size and thus reduce the computational load and generally improve correlation. However the limited search area and important surface changes occurring over one year do not allow to capture surface displacements for relatively fast-flowing areas of the land-terminating glaciers or the very fast tidewater glacier Jakobshavn Isbræ in the north of the study area (Fig. 1).

We use an automated calibration that takes advantage of ice velocity products from previous surveys (Mouginot et al., 2012, 2017). Offsets are first cleaned using a 9 × 9 pixels median filtering. Then the lowest speeds or ice-free areas are used for calibration. The calibration is performed by adjusting the difference between the reference map and the offset map with a constant value or a linear plane for Sentinel-2 and Landsat 8, respectively (Millan et al., 2019). The obtained velocity products are geocoded with the WGS 84 / NSIDC Sea Ice Polar Stereographic North projection (EPSG:3413) and re-sampled at a resolution of 150 m, similar to previous work (e.g. Derkacheva et al., 2020; Mouginot et al., 2017). With a revisiting time reduced from 16 days to 5 days with the launch of the Sentinel-2 constellation, our dataset is much richer from 2016, due to an increased number of image availability and combinations (Fig. 2). An overview of all yearly velocity maps obtained is displayed in Fig. 3, and all data is publicly available ([dataset] Halas et al., 2022, released 2022-12-09).

In addition, RMSE was calculated comparing obtained remotely-sensed velocities and ground-based measured velocity (Fig. 4).

2.3. GPS measurements

Ice velocity was measured by GPS on Isunnguata Sermia in West Greenland, from July 2014 to July 2017 (Maier et al., 2019).

We take advantage of the quasi-continuity of the GPS data, to check our satellite-based velocities, and to assess whether the starting date of an image pair or the baseline between images affects the obtained velocities.

From the GPS positions, ice velocity is estimated on a daily basis. The results highlights the enhanced and highly variable motion during the melt seasons and slow stable velocity during the winter months (Fig. 5) as already shown in Maier et al. (2019).

GPS measurements are not available during parts of the winters, therefore a linear interpolation was applied to complete the time series, which seems an appropriate approximation since winter velocities are not expected to differ significantly from a linear trend in the studied area (Derkacheva et al., 2020; Joughin et al., 2018; Van De Wal et al., 2015). To obtain comparable outputs from the GPS data and our feature-tracking derived velocities, we compute left-aligned moving averages on GPS velocities, with window sizes ranging from 336 days to 400 days, since the displacement observed between the two satellite images can be compared with the sum of daily displacements for the same time interval. Since we only used satellite observations acquired along the same orbits, the nominal cycles for Landsat 8 and Sentinel-2 are 16 and 5 days respectively. Based on this, the window sizes used were therefore chosen to be the same as duration between images used for feature-tracking, 368 days being the closest to yearly average for Landsat, and 336 and 400 days being the shortest and longest baseline used in our study. We compared the GPS moving averages with the remote sensing data at the same location, by plotting all the velocity data points obtained by

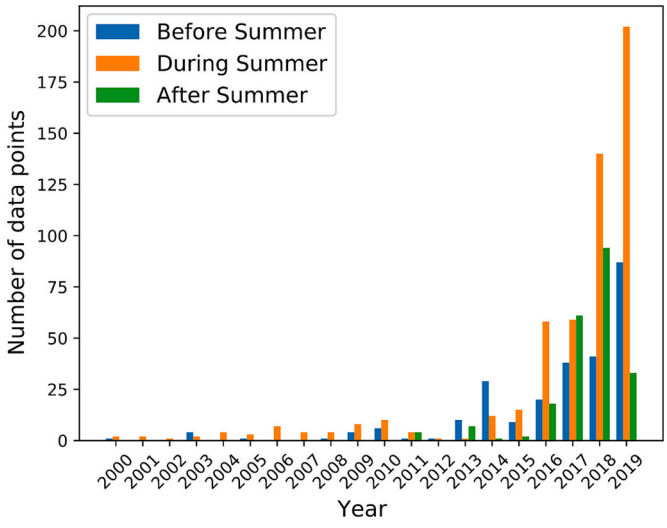

Fig. 2. Number of velocity data points according to the selection operated on the starting date, and at the same location as for the GPS study.

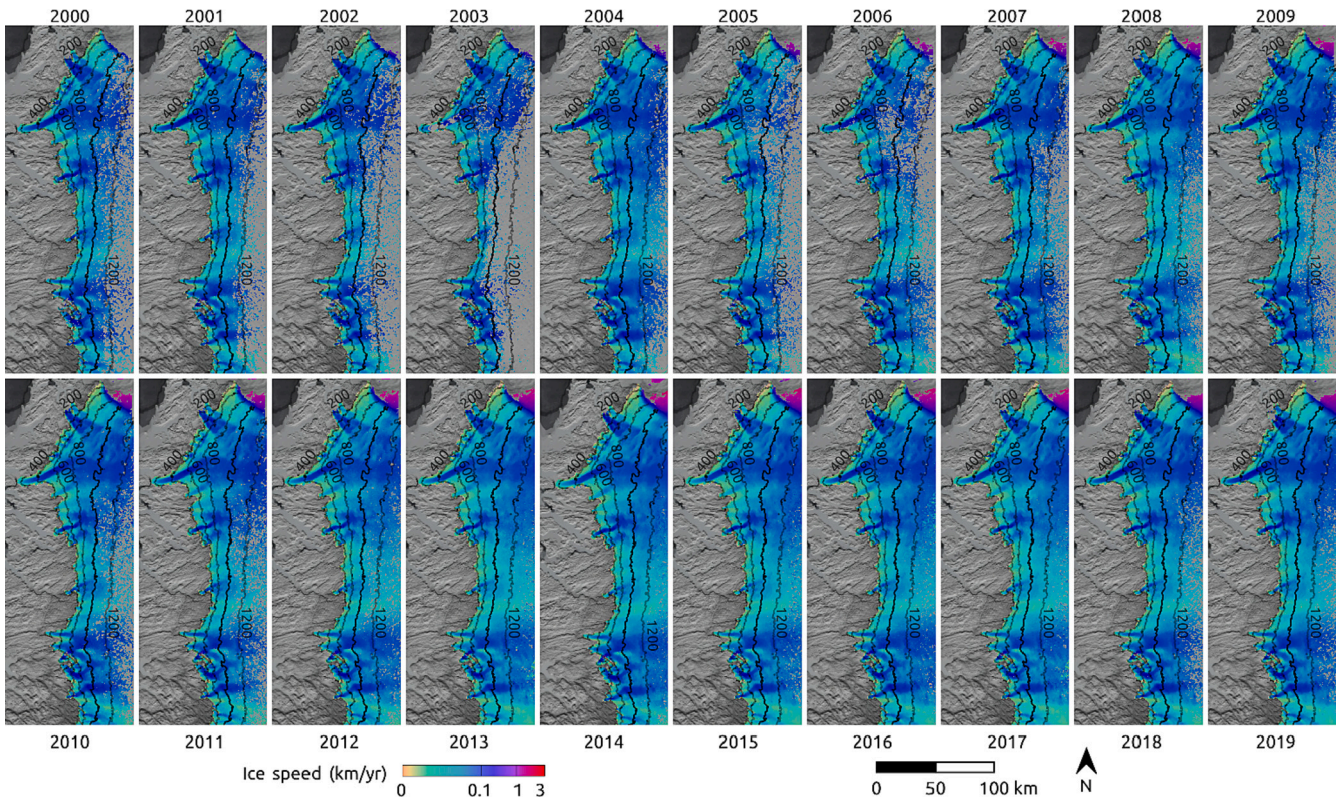

Fig. 3. Yearly velocity maps obtained in the study area between 2000 and 2019, averaging all velocities obtained with feature-tracking for every year.

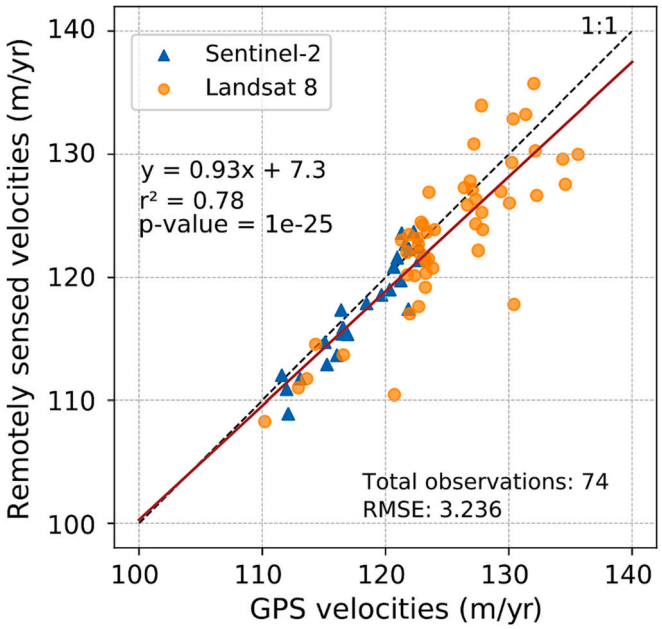

Fig. 4. Remotely sensed velocities plotted against GPS average over the corresponding period. The RMSE was calculated from all the values available.

feature-tracking for a given year (Fig. 6), as explained earlier. As a convention in our plots, the yearly average velocity for both GPS moving averages and feature-tracking measurements is plotted at the date at which the moving window or image pair starts.

2.4. Ice velocity trends

Least-square linear regressions are used to obtain ice velocity trends through time at each pixel, i.e. every 150 m. As a result, we obtain a trend map, where each trend is computed independently from other surroundings pixels. While Tedstone et al. (2015) and Williams et al. (2020) combined all their measurements into one set of annual velocity maps from which trends have been derived, we use both the combined dataset as well as split them into three subgroups representing different times of the year.

This temporal selection is done to determine the impact of the starting date on the trends. The groups are defined as follows:

- speed measurements whose first image is before summer (BS), i.e. in April and May
- speed measurements whose first image is during summer (DS), i.e. in June, July and August
- speed measurements whose first image is after summer (AS), i.e. September and October
- no temporal selection (ALL), i.e. all months are considered in the same way as for Tedstone et al. (2015) or Williams et al. (2020)

The BS and AS groups were chosen to avoid having two summer seasons in one measurement. Unfortunately, this division into four groups was only possible for years after 2012, as only a limited number of velocity measurements can be made at the GPS position before 2012 using Landsat 7. Indeed, only few measurements are available before the summer for the period 2000–2012 (Fig. 2).

The trend maps including all data (ALL) are computed for both periods 2000–2012 (Fig. 7) and 2012–2019 (Fig. 8). However, the sensitivity of the trends to the starting date is done by comparing the results for the groups BS, DS and AS, and can therefore only be made over the period 2012–2019 (Fig. 9).

We combine measurements from each group by taking the median

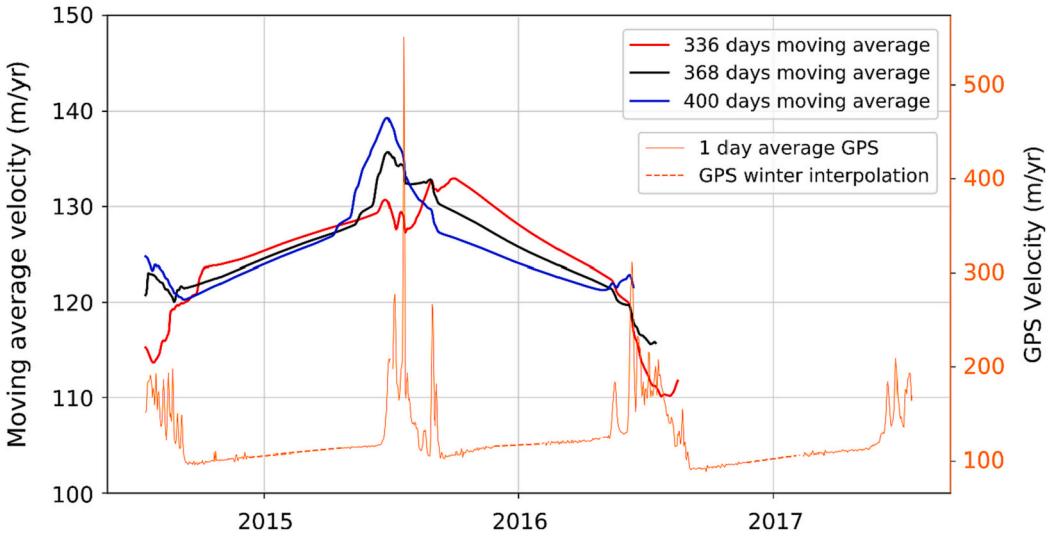

Fig. 5. Daily average GPS velocities (right orange axis, thin orange line (Maier et al., 2019), and moving average with window size varying between 336, 368 and 400 days (left axis, thicker lines). GPS daily ice velocities and moving averages are plotted on different axis because daily ice velocities display greater variations compared to moving yearly averages. As a convention in our plots, the yearly average velocity for GPS moving averages is plotted at the date at which the moving window starts.

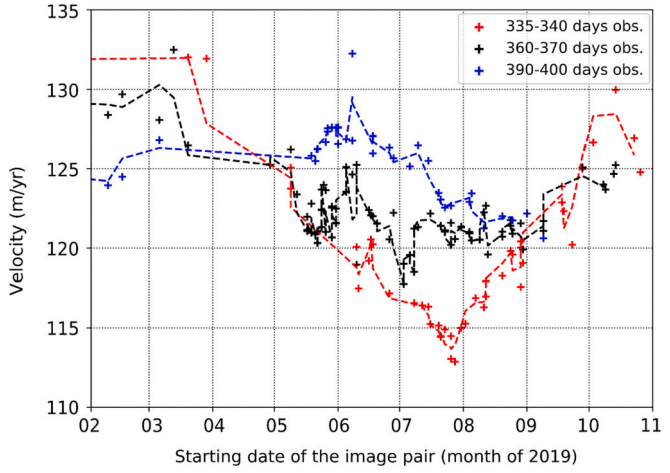

Fig. 6. Optical feature-tracking velocities from Landsat 8 and Sentinel-2 pairs, colored depending on the baseline between images. The dashed-line for each dataset represents a moving-average with size window 2. As a convention in our plots, the yearly average velocity for feature-tracking measurements is plotted at the date at which the image pair starts. The location is at the GPS point displayed in Fig. 1.

value at each pixel, resulting in four velocity maps for a given year, corresponding to the 4 groups BS, DS, AS and ALL.

For each group, we obtain the velocity trend as the slope of the linear regression, the *p*-value representing the significance of the trend and r^2 the coefficient of determination and the number of measurements used for the regression.

The number of available velocity data points every year for each pixel also varies. We notice that regressions where the number of measurements is too low performed badly. We therefore filter the trend maps where a low number of velocities are used to derive the trend, which was defined at 40% of the map per-pixel data points average.

This filtering was carefully chosen in order to eliminate all obvious outliers while preserving as much as possible the spatial coverage.

We also remove from the map all pixels we did not have a value for every year, except for the 2000–2012 period where year 2003 which had an insufficient spatial coverage compared to other years.

The trend map of the ALL group (without any time selection) is defined as the reference map in the rest of the study and serves as a point of comparison for the other trend maps of the BS, DS and AS groups (Fig. 9).

3. Results

3.1. Velocity maps from feature-tracking

After applying feature-tracking on all available satellite images, we obtain maps showing yearly averaged velocities (Fig. 3). The spatial coverage varies per year, depending on the amount of available images. After 2013, the coverage of our velocity maps improves with the launch of Landsat 8. Year 2003 has the least coverage of all maps from our dataset. All velocity maps clearly show the higher velocities of the glaciers, with velocities reaching above 150 m/yr, compared to other areas around flowing at speeds between 50 and 100 m/yr.

We computed the root mean squared error at the GPS location for overlapping period between GPS and remotely sensed velocities, by performing a GPS average for the exact same period for 74 single measurements, and the value found is around 3.2 m/yr (Fig. 4). There is a good agreement between satellite observations and the GPS. It appears that satellite data is more scattered for higher velocities, but this might be explained by a smaller number of data for smaller velocities. Due to the mission start of Sentinel-2 after the GPS deployment, there is no overlap of Sentinel-2 with the GPS for faster velocities, not allowing comparison between the satellites at this range of velocities.

3.2. Impact of starting date and baseline duration on velocities

Due to the deployment period of the GPS, our moving averages completely cover winter season 2014, melt season 2015 and following winter 2015. Melt season of 2014 and 2016 are, however, only partially covered.

Fig. 5 shows that both the starting date and the baseline duration have an effect on the calculated average velocity. The average velocity obtained for each window size is not constant throughout the year, and this evolution is different when the baseline is shortened or lengthened.

The variations between baseline duration are greater in summer than in winter. The 3 baselines seem to be closer in winter, with the closest values just before the melt season in April or May.

As the starting date of the moving average approaches the melt season, the results obtained for the different baselines are very different.

The data averaged over 400 days, i.e. more than one year, varies more during the year and reaches a higher value during the summer than those averaged over 336 or 368 days. This is due to an over-representation of the summer months compared to the winter months

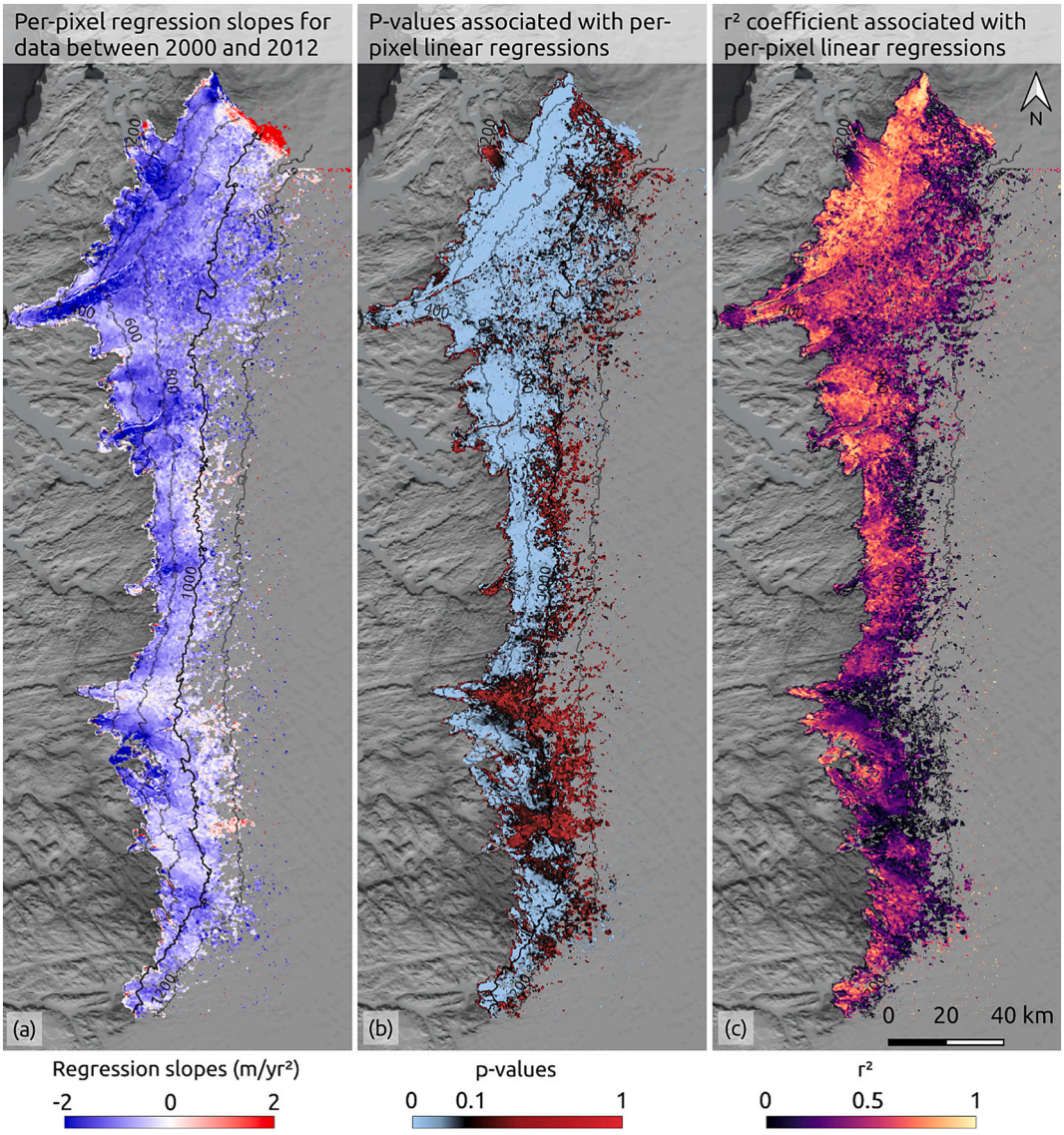

Fig. 7. (a) Map displaying the linear regression slopes for our study area, computed for each pixel on data from 2000 to 2012; (b) Map of the associated *p*-values; (c) Map of the associated r^2 coefficients.

in the 400-day average. Conversely, during the winter months, an over-representation of the winter months compared to the summer months results in a lower average speed for the longer baselines compared to the shorter ones.

Using recent satellite imagery on year 2019 where the sampling frequency is very high (Fig. 2), we observe similar patterns and evolution of velocities depending on baseline and starting date (Fig. 6). Similar results are obtained for previous years, with 390–400 days baseline velocities being higher in summer than 360–370 days baseline, and 335–340 days showing slower velocities during summer than longer baselines.

As with the GPS observations, we find that the different baselines yield similar velocity averages right before and after the melt season. The differences observed are well above the expected and estimated noise level, and can reach between 10% and 15% of differences between the lowest sampled velocity and the highest sampled velocity, compared to an annual average sampled before the melt season.

The analysis of the GPS and feature-tracking velocities clearly shows the strong impact of seasonal variations on the annual averages. Thus, depending on the starting date and the baseline duration of the image pairs, the annual averages can vary significantly and can therefore have a potential impact of multi-annual velocity trends.

3.3. Velocity trends

The regression map combining all measurements (ALL) between 2000 and 2012 displays a general pattern of deceleration across our study area (Fig. 7a), with the exception of the northernmost part. This northern acceleration is the signature of retreat of Jakobshavn Isbrae (Joughin et al., 2008, 2020), which is outside of the scope of this study (displaying a different behavior, and being ocean-terminating glacier). In addition, our parameters for feature-tracking are specifically set for better correlation on land-terminating glaciers, and therefore do not provide a complete velocity field for such a fast glacier.

The *p*-values associated with the linear regressions indicate that trends are in vast majority extremely significant (p-value under 0.001, Fig. 7b), and the r^2 coefficients are approaching the value 1, giving confidence in the robustness of the linearly decreasing trends (Fig. 7c). The exception to this are places where the p-value is over the 0.1 significant threshold and where r^2 coefficient tends toward 0. These places where the trends are insignificant are generally located at or above the 1000 m contour altitude. Indeed, above this altitude, feature-tracking

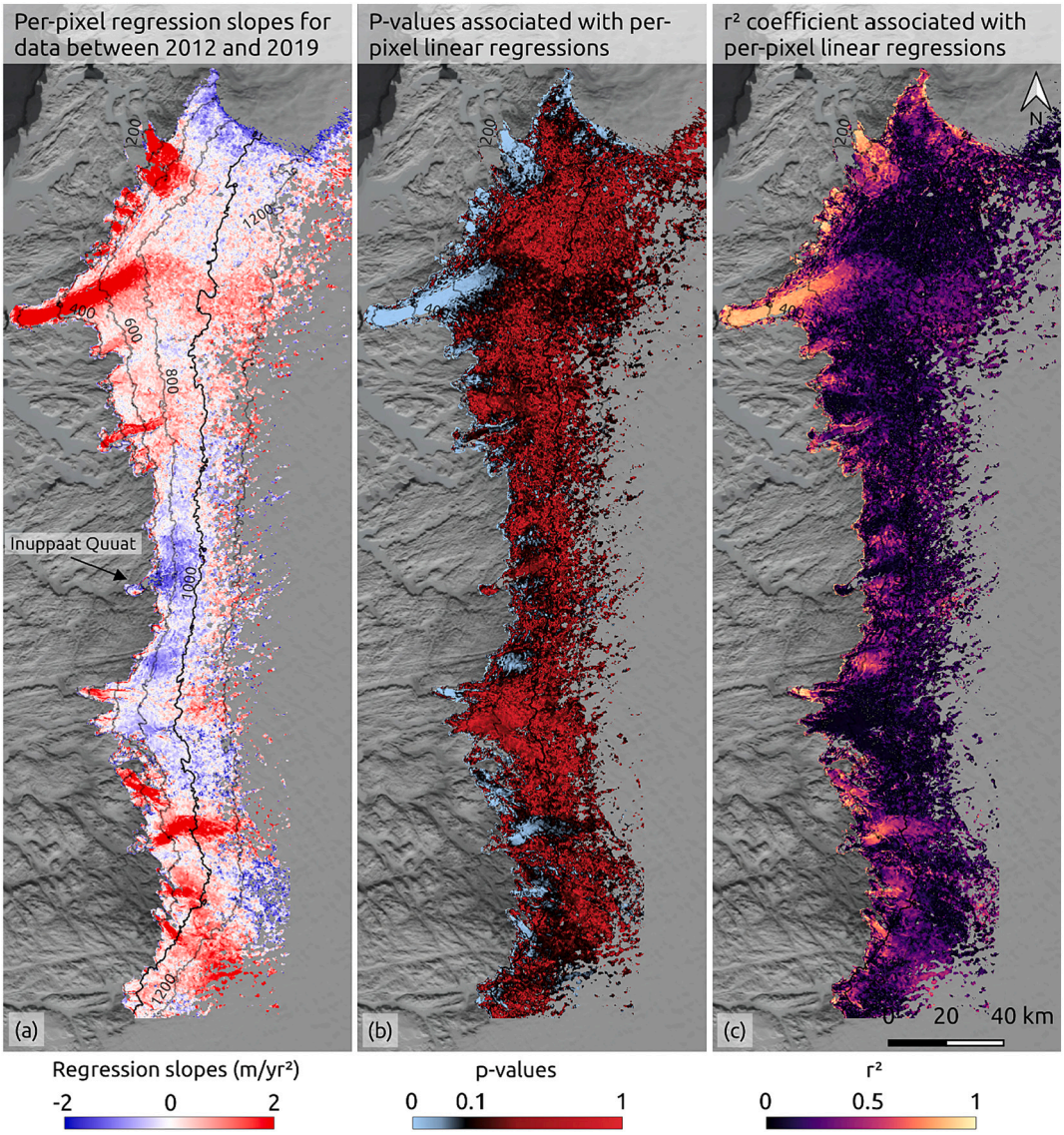

Fig. 8. (a) Map displaying the linear regression slopes for our study area, computed for each pixel on data from 2012 to 2019; (b) Map of the associated p-values; (c) Map of the associated r^2 coefficients.

tends to fail since the area undergoes less melting and remains mostly snow covered, limiting the presence of surface features that the cross-correlation algorithm can track. For the same reasons, almost no velocity tracking is possible above 1200 m in altitude.

The regression map (ALL) combining all speed measurements made during the period between 2012 and 2019 shows a more contrasting pattern of acceleration and deceleration (Fig. 8a) than the one for the period 2000–2012. In the central part of our study area near Inuppaat Quuat, ice velocity has been decelerating, as well as the northernmost part of our study area, while the rest mostly either accelerated, or did not display any significant variation in velocity. Indeed, the associated *p*-value map shows that most of the trends observed are weakly ($p \sim 0.05$) or non-significant (>0.1) (Fig. 8b). It appears that only the faster parts of our study area (Nordenskiöld Gletscher, Saqqarliup Sermia and Alangorliup Sermia in north and south of Russel Gletscher) are displaying acceleration with significant *p*-values and r^2 coefficients approaching 1 (Fig. 8c).

When computing regression maps for the different groups of data, we observe that all three groups of data (BS, DS, AS) display differences in velocities compared to the reference map (ALL) (Fig. 9).

Taking data from before summer (BS) shows less accelerating patterns compared to the reference map (ALL), and in the center of our study area around and south of Inuppaat Quuat we find a more pronounced slowdown. Nordenskiöld Gletscher tongue is also found to be accelerating in the (BS) map, but the surroundings display slightly decelerating trends compared to the reference map (ALL). The most negative trends are found above 800 m of Usulluup Sermia, and are not really observed on the reference map (ALL) (Fig. 9b).

The DS regression map appears on the opposite to be displaying more accelerating trend than the reference map (Fig. 9c). The deceleration trend found around Inuppaat Quuat for the reference map (ALL) is not as pronounced for the DS map.

The AS regression map is displaying more trends toward deceleration compared to the reference map, but not as much as the BS map (Fig. 9d). The south of Russel Gletscher appears also to be decelerating using AS data, a trend that is not observed using ALL data.

In the relatively fast-flowing area of Nordenskiöld Gletscher, data is missing for some maps, even though we usually obtained a better spatial coverage for low altitude ice in the rest of the map.

The reason is the parameters chosen for the feature-tracking when optimizing toward slower velocities: since we found better correlation for the overall area with smaller search window, we used this parameter

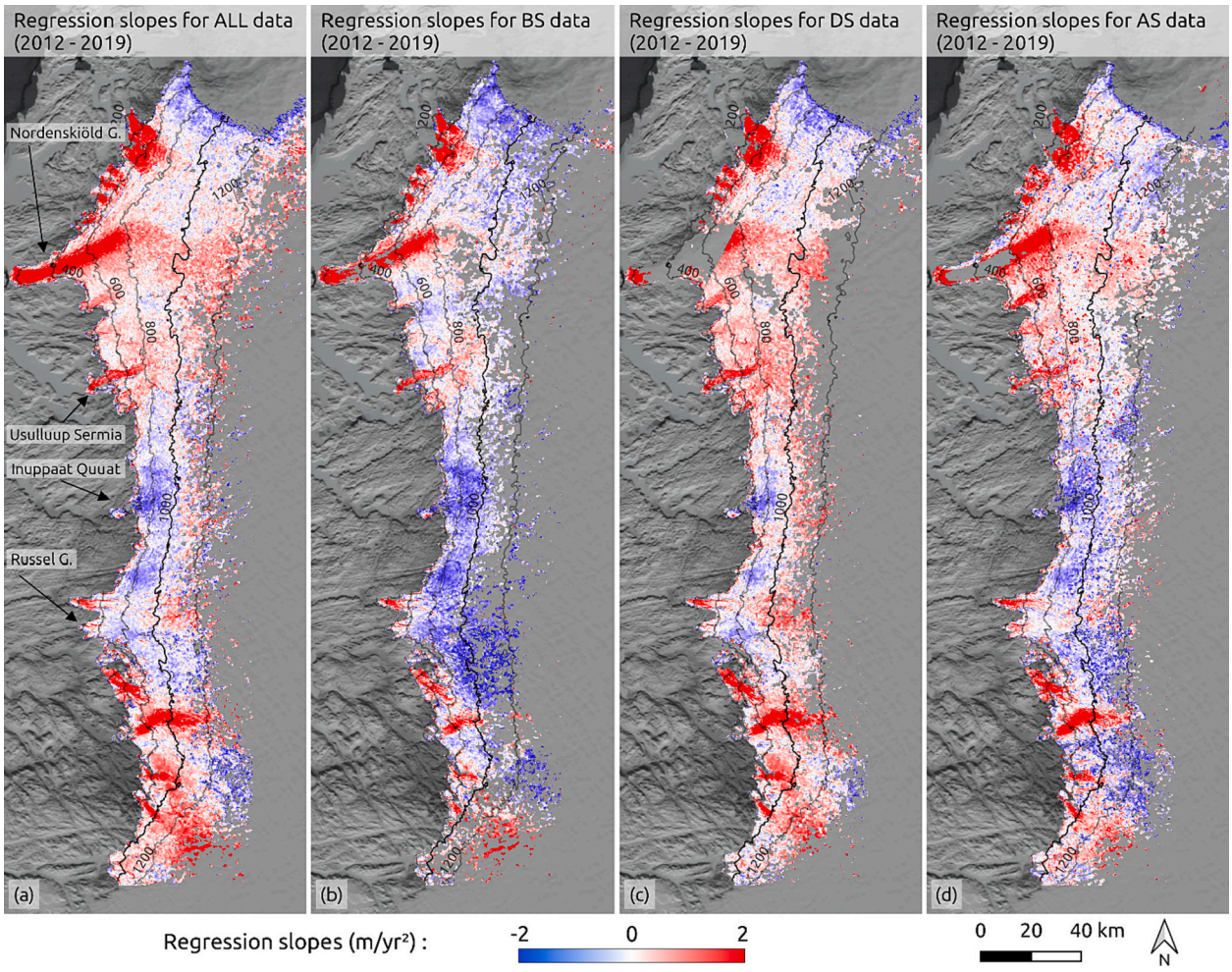

Fig. 9. (a) Map displaying the velocity trends computed for each pixel using all data from 2012 to 2019 (reference map); (b) Velocity trends using only before summer (BS) data; (c) Velocity trends using only during summer (DS) data; (d) Velocity trends using only after summer (AS) data. All for the period 2012 to 2019.

on the whole region and therefore have fewer data points in this faster flowing area. The affected pixels were then filtered out because the number of data points was below the threshold, as explained in Method 2.4.

Concluding, both the GPS dataset and the Satellite observations time series (Fig. 5 and Fig. 6) show that depending on the baseline duration and the start date, the obtained average velocity can vary between 10% and 15%.

The different regression maps display differences depending on the starting date, implying that the sampling of data is not only impacting velocity averages, but also translates into an impact on trends.

4. Discussion

4.1. Image pair temporal baseline and start date impact

For both moving averages on GPS data and satellite observations, differences in the annual velocities can be observed depending on the starting date and the baseline duration (Fig. 5, Fig. 6). This can be explained by the temporal baseline duration between images, and the percentage of summer velocities included in the average. When the starting date is close to the melt season and the baseline duration is longer than a year, the velocity measurement includes both the current and next year's melt season, resulting in faster average velocity. The opposite occurs with the shorter baselines: when the starting date is during the melt season and the baseline is shorter than one year, it only partially captures the current melt season and stops before the following one. In this latter case, the relative importance of winter velocities in the average is greater, leading to a slower average speed. Similarly, long baselines with a starting date during winter captures more winter velocities, inducing slower speed.

We show here that average velocities with their starting date during summer are dependent on both the current year melt season and on the following year melt season, and argue that they are therefore to a lesser extent representative of the current year ice velocity. We also argue that including next year's melt season may cause comparisons between different combinations of temporal baselines and starting date to be erroneous, since the averages compared will not be representing the same period of the year. We however observed that differences between velocities derived from image pairs with different baseline duration is limited before the melt season. Since the objective is still to obtain the best spatial coverage, this time period less prone to variations between baselines could be used to take advantage of multiple image pairs, while gaining representativeness in yearly velocities (Fig. 5).

Our findings therefore suggests that velocity trends should be done on velocities with image pairs starting before summer, including therefore for a given year, the melt season plus the following winter.

4.2. Velocity trends

When observing velocity trends on the whole region, the values for trends obtained for 2000–2012 are displaying a deceleration, similar to

previous studies (Tedstone et al., 2015; Williams et al., 2020) (Fig. 7a). While Tedstone et al. (2015) found a deceleration trend for the area of -1.5 m/yr^2, and Williams et al. (2020) found -1.64 m/yr^2, we find a decelerating trend of -1.13 m/yr^2, closer to Joughin et al. (2018) value found for a part of Tedstone et al. (2015) area, with a decelerating trend around -1.2 m/yr^2. This new value is not directly comparable with Tedstone et al. (2015) and Williams et al. (2020) values since the new value given here is a median of all single statistically significant ($p < 0.1$) per-pixel linear regression velocity trends, while previous values were obtained with a single linear regression for the period and on the whole area.

Also, Williams et al. (2020) did use pixels exclusively below 1000 m. Since in our 2000–2012 map we have a few pixels with velocities above 1000 m, we recomputed the region decelerating trend excluding pixels above 1000 m, and found almost the exact same value, varying only after the third digit. Also, the time interval is not exactly the same since we decided to start our trends in 2000 to gather more data. We present here the map with the per-pixel linear regression slopes used for calculation of the study area velocity trend, instead of a difference map like previously done in Tedstone et al. (2015) and Williams et al. (2020), and find that the deceleration trend seems robust and widespread across the area over the period 2000 to 2012 (Fig. 7b).

Joughin et al. (2018) did find a small area included in the Tedstone et al. (2015) study area where decelerating trends were observed, but concluded that this was an exception to Tedstone et al. (2015) area.

For the period 2012–2019, we find significant positive regression slopes (acceleration) on low lying glaciers tongue, but velocity trends elsewhere are generally insignificant and not spatially.

consistent. We therefore do not find the region-wide re-acceleration pattern over 2012–2019 found by Williams et al. (2020) (Fig. 8a).

This suggests that giving an average trend on the whole area may hide more complex local ice behaviors, and that per-pixel linear regressions should be performed instead.

Since Tedstone et al. (2015) and Williams et al. (2020) did not use a combination of Sentinel-2 and Landsat images as done here, we recomputed a per-pixel linear regressions map using only Landsat images (map provided in Fig. S1 in Supplementary Information), and observed almost no difference between maps using either one or both sensors for regression maps (Fig. S1 a,b), and for associated *p*-value maps (Fig. S1 c,d). This allows us to confirm that the difference observed between results from Williams et al. (2020) and our results is not due to the use of different sensors.

Finally, when computing *p*-values associated to our trends in the 2012–2019 period, most trends on the map are not statistically significant (Fig. 8b). This could be explained by a weak statistical power due to a short period of time (8 years) or by a mismatch between complex ice behavior observed and the simple linearity of the least-square linear regression model chosen to explain observations. This nevertheless reinforces the importance of displaying p-value maps associated with per-pixel linear regressions instead of map-wide linear regressions.

The only region with statistically significant trends show large acceleration on glacier tongues, which could potentially drive the positive trend found by Williams et al. (2020). We are not confident interpreting the spatial patterns of significance found, as trends found for fast flowing ice might be significant due to faster velocities and thus, greater observed differences. In addition, a few more years of data may confirm or refute the trends observed, or may reveal a new breakpoint, such as the one around 2012 found earlier by Williams et al. (2020), that was not found in Tedstone et al. (2015) dataset stopping in 2014.

Joughin et al. (2018) did not find significant deceleration trends in the low-lying glacier tongue, where we found a significant reacceleration between 2012 and 2019.

Differences in the results observed in these areas could therefore be due to the differences in time intervals for the per-pixel linear regression, which was in Joughin et al. (2018) between 2000–2001 and 2016–2017. In addition to this, methodology differences that could lead to such different findings in Joughin et al. (2018) could be related to the use of winter scenes, the number of years sampled that is lower in Joughin et al. (2018) due to winter scene availability between 2001 and 2017, and the sampling of winter scenes used to obtain velocities.

Joughin et al. (2018) uses velocity averages spanning over varying winter months (between October and April), period that can vary depending on the data availability. Even though the issue of varying sampling was addressed in Joughin et al. (2018), winter ice motion could display different behavior in different areas of our study region, and be varying enough such that the sampling of winter scenes affects trends observed more than previously thought.

For comparison purposes with previous work done by Williams et al. (2020), we also performed per-pixel percentage velocity differences between 2012 and 2019 (Fig. S2 in Supplementary Information), and found an acceleration pattern on most of the area as found by Williams et al. (2020). We however still argue for per-pixel linear regressions that encompass more data and describe more accurately ice velocity trends in the region.

4.3. Impact of image pair selection on trend maps

The maps with different datasets for the period 2012–2019 show that the selection of the starting date has consequences on the obtained trends (Fig. 9). The results also show that the deviations between maps are heterogeneous and vary by region and altitude. For every image pair, feature-tracking is potentially yielding a different spatial extent of where features could be tracked. Both Tedstone et al. (2015) and Williams et al. (2020) did use a common set of subset of pixels on which a value was obtained for every year, but the combination of image pairs used to obtain an average velocity at each pixel may be different if no control is applied to which image is used at every pixel and every year. Therefore, by combining all possible data as done in Tedstone et al. (2015) and Williams et al. (2020), there is a risk to obtain an unbalanced representation of the year, that will be different for every year and for every pixel, and this is particularly true for years before the launch of Landsat 8 due to an increase availability of optical images during summer.

We also observed here that even with a rich dataset (2012–2019), combining numerous velocity data points for each pixel still lead to differences in trends between groups, indicating that combining an increase number of velocity data is not sufficient to obtain comparable yearly velocities (Fig. 9).

Combining these results with the previous part, we argue that we should use image pairs starting before summer when that is applicable to avoid any comparison incompatibility between years.

The differences between maps found here are only representative of the time interval for which the trends were derived (2012–2019) and it is not possible to directly transpose our results for earlier dataset, where velocity trends are different. We however expect that this result holds for preceding periods as the effect is mostly due to the seasonality of velocities. This analysis is only possible due to numerous velocity measurements made with recent satellites, and cannot be done with such precision for years before the launch of Landsat 8. However, when possible, it is critical to sample annual velocities using comparable data, i.e., image pairs representing a similar time interval for each year.

5. Conclusion

In our study, we find a decelerating velocity trend for the period 2000–2012 as observed by Tedstone et al. (2015) and Williams et al. (2020), in the Southwest of the Greenland Ice Sheet, on a larger area extending South of the previous studies. While the velocity trends found for each pixel of the region for 2000–2012 are mostly decelerating, the velocity trend maps for 2012–2019 display both positive and negative velocity trends. This implies that giving an average acceleration estimate for the whole region is not correctly depicting the behavior of the ice sheet in this area, and that local velocity trend behaviors will be

hidden if we assume that the whole area has a similar behavior.

This is reinforced by our *p*-value map, displaying that most per-pixel linear regressions are not significant for the last period, while Williams et al. (2020) were still able to find a significant trend when combining all pixels to perform a linear regression on velocities to describe the whole area. Unlike Tedstone et al. (2015) and Williams et al. (2020), we display maps with per-pixel linear regressions, and we argue that this should be done in order to see potential local behaviors as found here. These local differences in velocity trend can be missed otherwise, but are necessary to better understand the relation between surface melting and ice velocities. Trends must also be computed for each pixel, and not on the median of all pixels in the area.

Concerning the image pairs used to obtain yearly ice velocities, a one year baseline is commonly used to avoid strong seasonal variations. However, we show that differences can still be observed when comparing velocities derived either from image pairs that do not have the same starting date, or that have a different baseline duration between images. We do find differences in a yearly average whether the start date is before summer, during summer or after summer, as clearly shown on both the GPS dataset and with satellite observations. We also found that the baseline duration has a reduced impact if the start date is before summer, and has a maximum impact if the start date is during summer, being explained by the presence of the following summer velocities in the average when using pairs starting during summer. We were unable to perform different linear regression maps depending on the starting date on 2000–2012 due to lack of data, but differences were observed on the 2012–2019 dataset when using different starting dates to compute yearly ice velocity average. We acknowledge that the data, particularly before 2000 with Landsat 5, did not allow to perform such per-pixel linear regression, due to the limited number of images with sufficient quality.

Recent satellite launches now allow us to precisely select the starting dates and baseline duration without compromising on the spatial coverage, thanks to increased temporal resolution.

We therefore argue that, when possible, image pairs starting before summer should be used to draw accurate trends on velocities, so that yearly velocities obtained represent as much as possible the same velocity averages, in order to be compared. This is especially important when observed trends are relatively small compared to the amplitude of the signal. Such description of velocity trend, more accurate and on a more local scale, is required to understand and better assess the impact of future surface melting on ice sheet dynamics.

Supplementary data to this article can be found online at https://doi.org/10.1016/j.rse.2022.113419.

Acknowledgement and Financial support

We would like to thank Nathan Maier for providing access to the GPS data.

This work is part of the SWItchDyn project funded by the Research Council of Norway (NFR-287206) and the Bjerknes Centre for Climate Research strategic project RISES. Computing was performed on the resources provided by UNINETT Sigma2 – the National Infrastructure for High Performance Computing and Data Storage in Norway (NN9635K and NS9635K).

CRediT authorship contribution statement

Paul Halas: Methodology, Software, Validation, Formal analysis, Investigation, Data curation, Writing – original draft, Writing – review & editing, Visualization. **Jérémie Mouginot:** Conceptualization, Methodology, Software, Validation, Formal analysis, Data curation, Writing – review & editing, Supervision. **Basile de Fleurian:** Conceptualization, Methodology, Validation, Formal analysis, Resources, Writing – review & editing, Supervision, Funding acquisition. **Petra M. Langebroek:** Methodology, Validation, Writing – review & editing, Supervision.

Declaration of Competing Interest

The authors declare that they have no known competing financial interests or personal relationships that could have appeared to influence the work reported in this paper.

Data availability

The velocity products derived from optical-feature tracking for this study are published in "Southwest Greenland Ice Sheet Yearly Ice Velocities dataset from 1984 to 2020" DOI: 10.5281/zenodo.7418361

References

Bougamont, M., Christoffersen, P., Hubbard, A.L., Fitzpatrick, A.A., Doyle, S.H., Carter, S.P., 2014. Sensitive response of the Greenland ice sheet to surface melt drainage over a soft bed. Nat. Commun. 5, 1–9. https://doi.org/10.1038/ncomms6052.

Brinkerhoff, D., Aschwanden, A., Fahnestock, M., 2021. Constraining subglacial processes from surface velocity observations using surrogate-based Bayesian inference. J. Glaciol. 67, 385–403. https://doi.org/10.1017/jog.2020.112.

Halas, P., Mouginot, J., de Fleurian, B., Langebroek, P., 2022. Southwest Greenland Ice Sheet Yearly Ice Velocities dataset from 1984 to 2020. https://doi.org/10.5281/zenodo.7418361 [dataset].

Davison, B.J., Sole, A.J., Livingstone, S.J., Cowton, T.R., Nienow, P.W., 2019. The influence of hydrology on the dynamics of land-terminating sectors of the Greenland ice sheet. Front. Earth Sci. https://doi.org/10.3389/feart.2019.00010.

de Fleurian, B., Morlighem, M., Seroussi, H., Rignot, E., van den Broeke, M.R., Kuipers Munneke, P., Mouginot, J., Smeets, P.C.J.P., Tedstone, A.J., 2016. A modeling study of the effect of runoff variability on the effective pressure beneath Russell glacier, West Greenland. J. Geophys. Res. Earth Surf. 121, 1834–1848. https://doi.org/10.1002/2016JF003842.

Debella-Gilo, M., Kääb, A., 2011. Sub-pixel precision image matching for measuring surface displacements on mass movements using normalized cross-correlation. Remote Sens. Environ. 115, 130–142. https://doi.org/10.1016/j.rse.2010.08.012.

Dehecq, A., Gourmelen, N., Gardner, A.S., Brun, F., Goldberg, D., Nienow, P.W., Berthier, E., Vincent, C., Wagnon, P., Trouvé, E., 2019. Twenty-first century glacier slowdown driven by mass loss in High Mountain Asia. Nat. Geosci. 12, 22–27. https://doi.org/10.1038/s41561-018-0271-9.

Dehecq, A., Gourmelen, N., Trouve, E., 2015. Deriving large-scale glacier velocities from a complete satellite archive: application to the Pamir-Karakoram-himalaya. Remote Sens. Environ. 162, 55–66. https://doi.org/10.1016/j.rse.2015.01.031.

Derkacheva, A., Mouginot, J., Millan, R., Maier, N., Gillet-Chaulet, F., 2020. Data reduction using statistical and regression approaches for ice velocity derived by Landsat-8, Sentinel-1 and Sentinel-2. Remote Sens. 12, 1935. https://doi.org/10.3390/rs12121935.

Dow, C.F., Hubbard, A., Booth, A.D., Doyle, S.H., Gusmeroli, A., Kulessa, B., 2013. Seismic evidence of mechanically weak sediments underlying Russell glacier, West Greenland. Ann. Glaciol. 54, 135–141. https://doi.org/10.3189/2013AoG64A032.

Doyle, S.H., Hubbard, A., Fitzpatrick, A.A.W., van As, D., Mikkelsen, A.B., Pettersson, R., Hubbard, B., 2014. Persistent flow acceleration within the interior of the Greenland ice sheet. Geophys. Res. Lett. 41, 899–905. https://doi.org/10.1002/2013GL058933.

Fahnestock, M., Scambos, T., Moon, T., Gardner, A., Haran, T., Klinger, M., 2016. Rapid large-area mapping of ice flow using Landsat 8. Remote Sens. Environ. 185, 84–94. https://doi.org/10.1016/j.rse.2015.11.023.

Haran, T., Bohlander, J., Scambos, T., Painter, T., Fahnestock, M., 2018. MEaSUREs MODIS mosaic of Greenland (MOG) 2005, 2010, and 2015 image maps, version 2. National Snow and ice data center.

Harper, J.T., Humphrey, N.F., Meierbachtol, T.W., Graly, J.A., Fischer, U.H., 2017. Borehole measurements indicate hard bed conditions, Kangerlussuaq sector, western Greenland ice sheet. J. Geophys. Res. Earth Surf. 122, 1605–1618. https://doi.org/10.1002/2017JF004201.

Jeong, S., Howat, I.M., Ahn, Y., 2017. Improved multiple matching method for observing glacier motion with repeat image feature tracking. IEEE Trans. Geosci. Remote Sens. 55, 2431–2441. https://doi.org/10.1109/TGRS.2016.2643699.

Joughin, I., 2002. Ice-sheet velocity mapping: a combined interferometric and speckle-tracking approach. Ann. Glaciol. 34, 195–201. https://doi.org/10.3189/172756402781817978.

Joughin, I., Das, S.B., King, M.A., Smith, B.E., Howat, I.M., Moon, T., 2008. Seasonal speedup along the western flank of the Greenland ice sheet. Science 320, 781–783. https://doi.org/10.1126/science.1153288.

Joughin, I.E., Shean, D.E., Smith, B., Floricioiu, D., 2020. A decade of variability on Jakobshavn Isbræ: Ocean temperatures pace speed through influence on mélange rigidity. Cryosphere 14, 211–227. https://doi.org/10.5194/tc-14-211-2020.

Joughin, I., Smith, B.E., Howat, I., 2018. Greenland ice mapping project: ice flow velocity variation at sub-monthly to decadal timescales. Cryosphere 12, 2211–2227. https://doi.org/10.5194/tc-12-2211-2018.

Koziol, C.P., Arnold, N., 2018. Modelling seasonal meltwater forcing of the velocity of land-terminating margins of the Greenland ice sheet. Cryosphere 12, 971–991. https://doi.org/10.5194/tc-12-971-2018.

Koziol, C.P., Arnold, N., 2017. Incorporating modelled subglacial hydrology into inversions for basal drag. Cryosphere 11, 2783–2797. https://doi.org/10.5194/tc-11-2783-2017.

Kulessa, B., Hubbard, A.L., Booth, A.D., Bougamont, M., Dow, C.F., Doyle, S.H., Christoffersen, P., Lindbäck, K., Pettersson, R., Fitzpatrick, A.A.W., Jones, G.A., 2017. Seismic evidence for complex sedimentary control of Greenland Ice Sheet flow. Sci. Adv. 3 https://doi.org/10.1126/sciadv.1603071.

Lemos, A., Shepherd, A., McMillan, M., Hogg, A.E., 2018. Seasonal variations in the flow of land-terminating glaciers in central-West Greenland using Sentinel-1 imagery. Remote Sens. 10, 1–12. https://doi.org/10.3390/rs10121878.

Lilien, D.A., Joughin, I., Smith, B., Shean, D.E., 2018. Changes in flow of Crosson and Dotson ice shelves, West Antarctica, in response to elevated melt. Cryosphere 12, 1415–1431. https://doi.org/10.5194/tc-12-1415-2018.

Maier, N., Humphrey, N., Harper, J., Meierbachtol, T., 2019. Sliding dominates slow-flowing margin regions,Greenland Ice Sheet. Sci. Adv. 5 https://doi.org/10.1126/sciadv.aaw5406.

Millan, R., Mouginot, J., Rabatel, A., Jeong, S., Cusicanqui, D., Derkacheva, A., Chekki, M., 2019. Mapping surface flow velocity of glaciers at regional scale using a multiple sensors approach. Remote Sens. 11, 2498. https://doi.org/10.3390/rs11212498.

Millan, R., Mouginot, J., Rabatel, A., Morlighem, M., 2022. Ice velocity and thickness of the world's glaciers. Nat. Geosci. 15, 124–129. https://doi.org/10.1038/s41561-021-00885-z.

Moon, T., Joughin, I., Smith, B., 2015. Seasonal to multiyear variability of glacier surface velocity, terminus position, and sea ice/ice mélange in Northwest Greenland. J. Geophys. Res. Earth Surf. 120, 818–833. https://doi.org/10.1002/2015JF003494.

Mouginot, J., Rignot, E., Bjørk, A.A., van den Broeke, M., Millan, R., Morlighem, M., Noël, B., Scheuchl, B., Wood, M., 2019. Forty-six years of Greenland ice sheet mass balance from 1972 to 2018. Proc. Natl. Acad. Sci. U. S. A. https://doi.org/10.1073/pnas.1904242116.

Mouginot, J., Rignot, E., Scheuchl, B., Millan, R., 2017. Comprehensive annual ice sheet velocity mapping using Landsat-8, Sentinel-1, and RADARSAT-2 data. Remote Sens. 9, 1–20. https://doi.org/10.3390/rs9040364.

Mouginot, J., Scheuch, B., Rignot, E., 2012. Mapping of ice motion in Antarctica using synthetic-aperture radar data. Remote Sens. 4, 2753–2767. https://doi.org/10.3390/rs4092753.

Palmer, S., Shepherd, A., Nienow, P., Joughin, I., 2011. Seasonal speedup of the Greenland Ice Sheet linked to routing of surface water. Earth Planet. Sci. Lett. 302, 423–428. https://doi.org/10.1016/j.epsl.2010.12.037.

Parizek, B.R., Alley, R.B., 2004. Implications of increased Greenland surface melt under global-warming scenarios: ice-sheet simulations. Quat. Sci. Rev. 23, 1013–1027. https://doi.org/10.1016/j.quascirev.2003.12.024.

Paul, F., Bolch, T., Kääb, A., Nagler, T., Nuth, C., Scharrer, K., Shepherd, A., Strozzi, T., Ticconi, F., Bhambri, R., Berthier, E., Bevan, S., Gourmelen, N., Heid, T., Jeong, S., Kunz, M., Lauknes, T.R., Luckman, A., Merryman Boncori, J.P., Moholdt, G., Muir, A., Neelmeijer, J., Rankl, M., VanLooy, J., Van Niel, T., 2015. The glaciers climate change initiative: methods for creating glacier area, elevation change and velocity products. Remote Sens. Environ. 162, 408–426. https://doi.org/10.1016/j.rse.2013.07.043.

Rabatel, A., Ceballos, J.L., Micheletti, N., Jordan, E., Braitmeier, M., González, J., Mölg, N., Ménégoz, M., Huggel, C., Zemp, M., 2018. Toward an imminent extinction of Colombian glaciers? Geogr. Ann. Ser. Phys. Geogr. 100, 75–95. https://doi.org/10.1080/04353676.2017.1383015.

Rosen, P.A., Hensley, S., Peltzer, G., Simons, M., 2004. Updated repeat orbit interferometry package released. Eos Trans. Am. Geophys. Union 85, 47. https://doi.org/10.1029/2004EO050004.

Scambos, T.A., Dutkiewicz, M.J., Wilson, J.C., Bindschadler, R.A., 1992. Application of image cross-correlation to the measurement of glacier velocity using satellite image data. Remote Sens. Environ. 42, 177–186. https://doi.org/10.1016/0034-4257(92)90101-O.

Shen, Q., Wang, H., Shum, C.K., Jiang, L., Hsu, H.T., Dong, J., 2018. Recent high-resolution Antarctic ice velocity maps reveal increased mass loss in Wilkes Land, East Antarctica. Sci. Rep. 8, 1–8. https://doi.org/10.1038/s41598-018-22765-0.

Shepherd, A., Hubbard, A., Nienow, P., King, M., McMillan, M., Joughin, I., 2009. Greenland ice sheet motion coupled with daily melting in late summer. Geophys. Res. Lett. 36, L01501. https://doi.org/10.1029/2008GL035758.

Sole, A., Nienow, P., Bartholomew, I., Mair, D., Cowton, T., Tedstone, A., King, M.A., 2013. Winter motion mediates dynamic response of the Greenland Ice Sheet to warmer summers. Geophys. Res. Lett. 40, 3940–3944. https://doi.org/10.1002/grl.50764.

Tedstone, A.J., Nienow, P.W., Bartholomew, I.D., Sole, A.J., Cowton, T.R., Mair, D.W.F., King, M.A., 2013. Greenland ice sheet motion insensitive to exceptional meltwater forcing. Proc. Natl. Acad. Sci. U. S. A. 110, 19719–19724. https://doi.org/10.1073/pnas.1315843110.

Tedstone, A.J., Nienow, P.W., Gourmelen, N., Dehecq, A., Goldberg, D., Hanna, E., 2015. Decadal slowdown of a land-terminating sector of the Greenland Ice Sheet despite warming. Nature 526, 692–695. https://doi.org/10.1038/nature15722.

Tuckett, P.A., Ely, J.C., Sole, A.J., Livingstone, S.J., Davison, B.J., Melchior van Wessem, J., Howard, J., 2019. Rapid accelerations of Antarctic peninsula outlet glaciers driven by surface melt. Nat. Commun. 10, 1–8. https://doi.org/10.1038/s41467-019-12039-2.

Van De Wal, R.S.W., Boot, W., Van Den Broeke, M.R., Smeets, C.J.P.P., Reijmer, C.H., Donker, J.J.A., Oerlemans, J., 2008. Large and rapid melt-induced velocity changes in the ablation zone of the Greenland Ice Sheet. Science 321, 111–113. https://doi.org/10.1126/science.1158540.

Van De Wal, R.S.W., Smeets, C.J.P.P., Boot, W., Stoffelen, M., Van Kampen, R., Doyle, S.H., Wilhelms, F., Van Den Broeke, M.R., Reijmer, C.H., Oerlemans, J., Hubbard, A., 2015. Self-regulation of ice flow varies across the ablation area in south-west Greenland. Cryosphere 9, 603–611. https://doi.org/10.5194/tc-9-603-2015.

Williams, J.J., Gourmelen, N., Nienow, P., 2020. Dynamic response of the Greenland ice sheet to recent cooling. Sci. Rep. 10 https://doi.org/10.1038/s41598-020-58355-2.

Wright, P.J., Harper, J.T., Humphrey, N.F., Meierbachtol, T.W., 2016. Measured basal water pressure variability of the western Greenland ice sheet: implications for hydraulic potential. J. Geophys. Res. Earth Surf. 121, 1134–1147. https://doi.org/10.1002/2016JF003819.

Zhou, Y., Li, X., Zheng, D., Li, Z., An, B., Wang, Y., Jiang, D., Su, J., Cao, B., 2021. The joint driving effects of climate and weather changes caused the Chamoli glacier-rock avalanche in the high altitudes of the India Himalaya. Sci. China Earth Sci. 64, 1909–1921. https://doi.org/10.1007/s11430-021-9844-0.

Zwally, H.J., Abdalati, W., Herring, T., Larson, K., Saba, J., Steffen, K., 2002. Surface melt-induced acceleration of Greenland ice-sheet flow. Science 297, 218–222. https://doi.org/10.1126/science.1072708.